Pergamon

Geochimica et Cosmochimica Acta, Vol. 68, No. 22, pp. 4505-4518, 2004

0016-7037/04 $30.00 + .00

doi:10.1016/j.gca.2004.04.025

Adsorption of organic matter at mineral/water interfaces: I. ATR-FTIR spectroscopic and quantum chemical study of oxalate adsorbed at boehmite/water and corundum/water interfaces

TAE HYUN YOON,[1,*] STEPHEN B. JOHNSON,[1] CHARLES B. MUSGRAVE,[2] and GORDON E. BROWN, JR.[1,3]

[1]Surface & Aqueous Geochemistry Group, Department of Geological & Environmental Sciences, Stanford University, Stanford, California 94305-2115 USA
[2]Departments of Chemical Engineering and Materials Science & Engineering, Stanford University, Stanford, California 94305-5025 USA
[3]Stanford Synchrotron Radiation Laboratory, SLAC, 2575 Sand Hill Rd., MS 69, Menlo Park, California 94025 USA

(*Received September* 24, 2003; *accepted in revised form April* 23, 2004)

Abstract—The types and structures of adsorption complexes formed by oxalate at boehmite (γ-AlOOH)/water and corundum (α-Al_2O_3)/water interfaces were determined using *in situ* attenuated total reflectance fourier transform infrared (ATR-FTIR) spectroscopy and quantum chemical simulation methods. At pH 5.1, at least four different oxalate species were found at or near the boehmite/water interface for oxalate surface coverages (Γ_{ox}) ranging from 0.25 to 16.44 μmol/m^2. At relatively low coverages ($\Gamma_{ox} < 2.47$), strongly adsorbed inner-sphere oxalate species (IR peaks at 1286, 1418, 1700, and 1720 cm^{-1}) replace weakly adsorbed carbonate species, and a small proportion of oxalate anions are adsorbed in an outer-sphere mode (IR peaks at 1314 and 1591 cm^{-1}). IR peaks indicative of inner-sphere adsorbed oxalate are also observed for oxalate at the corundum/water interface at $\Gamma_{ox} = 1.4$ μmol/m^2. With increasing oxalate concentration ($\Gamma_{ox} > 2.47$ μmol/m^2), the boehmite surface binding sites for inner-sphere adsorbed oxalate become saturated, and excess oxalate ions are present dominantly as aqueous species (IR peaks at 1309 and 1571 cm^{-1}). In addition to these adsorption processes, oxalate-promoted dissolution of boehmite following inner-sphere oxalate adsorption becomes increasingly pronounced with increasing Γ_{ox} and results in an aqueous Al(III)-oxalate species, as indicated by shifted IR peaks (1286 $\rightarrow$ 1297 cm^{-1} and 1418 $\rightarrow$ 1408 cm^{-1}). At pH 2.5, no outer-sphere adsorbed oxalate or aqueous oxalate species were observed. The similarity of adsorbed oxalate spectral features at pH 2.5 and 5.1 implies that the adsorption mechanism of aqueous HOx^- species involves loss of protons from this species during the ligand-exchange reaction. As a consequence, adsorbed inner-sphere oxalate and aqueous Al(III)-oxalate complexes formed at pH 2.5 have coordination geometries very similar to those formed at pH 5.1.

The coordination geometry of inner-sphere adsorbed oxalate species was also predicted using quantum chemical geometry optimization and IR vibrational frequency calculations. Geometry-optimized Al_8O_{12} and $Al_{14}O_{22}$ clusters with the reactive surface Al site coordinated by three oxygens were used as model substrates for corundum and boehmite surfaces. Among the models considered, calculated IR frequencies based on a bidentate side-on structure with a 5-membered ring agree best with the observed frequencies for boehmite/oxalate/water samples at $\Gamma_{ox} = 0.25$ to 16.44 μmol/m^2 and pH 2.5 and 5.1, and for a corundum/oxalate/water sample at $\Gamma_{ox} = 1.4$ μmol/m^2 and pH 5.1. Based on these results, we suggest that oxalate bonding on boehmite and corundum surfaces results in 5-coordinated rather than 4- or 6-coordinated Al surface sites.

1. INTRODUCTION

Low molecular weight (LMW) carboxylic acids (e.g., oxalate, malonate, and citrate) are ubiquitous in natural environments (Strobel, 2001) and play important roles in soil and aqueous systems (Schnitzer, 2000). Due to their deprotonation at acidic to neutral pH, they typically exist in anionic forms in aqueous solutions, and therefore can easily adsorb onto positively charged mineral surfaces (e.g., aluminum- and iron-(oxyhydr)oxides) and result in significant changes in surface charge and metal ion adsorption capacities (Davis, 1982; Davis, 1984) and rates of mineral dissolution (Stumm, 1987; White and Brantley, 1995). Although extensive work has been done to identify the type(s) and structure(s) of surface complexes of relatively simple organic acids at mineral/water interfaces (Nordin et al., 1997; Nordin et al., 1998; Persson et al., 1998; Degenhardt and McQuillan, 1999; Dobson and McQuillan, 1999; Boily et al., 2000a; Axe and Persson, 2001; Duckworth and Martin, 2001), a molecular-level understanding of these interactions is not complete. In these studies, two major types of surface complexes have been suggested—inner-sphere mode with a direct bond between carboxylate oxygen and surface cations, and outer-sphere mode without any direct carboxylate oxygen-surface cation bond, and typically held at the surface through a combination of hydrogen bonding and electrostatic interactions. However, even for the simplest dicarboxylate compound such as oxalate, which is frequently assumed to form inner-sphere complexes at mineral/water interfaces (e.g., Furrer and Stumm, 1986; Axe and Persson, 2001), various coordination geometries are possible, including monodentate, mononuclear bidentate side-on, mononuclear bidentate end-on, and binuclear bidentate structures (Fig. 1). In these cases, different coordination structures may induce distinct charges

* Author to whom correspondence should be addressed (taeyoon@pangea.stanford.edu).

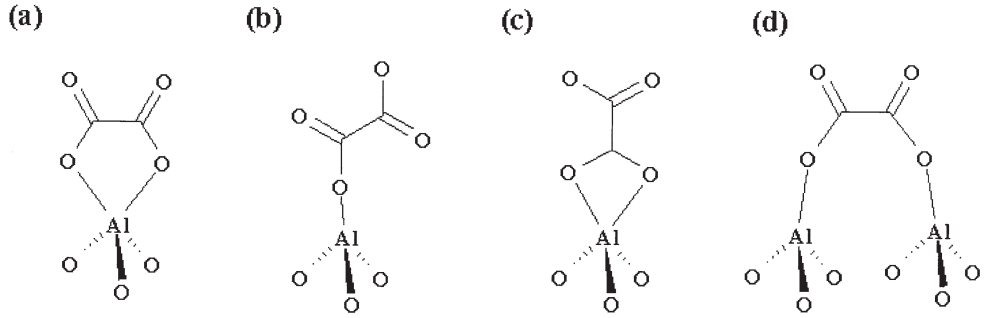

Fig. 1. Schematic drawing of four possible inner-sphere coordination structures for oxalate adsorbed at the Al-(oxyhydr)oxide/water interface: (a) mononuclear bidentate side-on coordination with 5-membered ring; (b) mononuclear monodentate end-on coordination; (c) mononuclear bidentate end-on coordination with 4-membered ring; and (d) binuclear bidentate coordination.

and reactivities at mineral/water interfaces, and consequently result in changes in the electrical double layer (Boily et al., 2000b). These changes, in turn, could induce changes in adsorption environments for other cationic and anionic species and could also enhance or inhibit mineral dissolution (Eick et al., 1999).

As part of a larger study of the interaction of simple as well as more complex naturally occurring organic compounds with mineral surfaces (see Johnson et al., 2004), we have examined the interaction of oxalate with boehmite (γ-AlOOH) and corundum (α-Al_2O_3) surfaces in the presence of bulk water at 25°C using a combination of *in situ* attenuated total reflectance FTIR spectroscopy and quantum chemical modeling. Oxalate is the smallest organic dicarboxylate ligand among the LMW organic compounds and is also one of the most abundant LMW organic acids in nature due to its secretion by plant roots, bacteria, and fungi in the rhizosphere (Vaughan and Wogelius, 2000; Strobel, 2001). In addition to its structural simplicity and natural abundance, oxalate also has a strong adsorption affinity for mineral surfaces and is known to catalyze mineral dissolution (Furrer and Stumm, 1986; Zinder et al., 1986). Aluminum (oxy)hydroxide (e.g., boehmite) is a common fine-grained constituent of soils and sediments due to its thermodynamic stability under hydrous conditions (Navrotsky, 2001). Boehmite is also an important industrial mineral used as a catalyst or catalyst support because of its ability to retain high surface area (Navrotsky, 2001). Corundum is an important model substrate for surface reactions, having been used as a sorbent in numerous metal ion sorption studies of importance in geochemistry and soil science (Brown and Parks, 2001). It is also an important metal oxide in the ceramics industry (Henrich and Cox, 1994). In addition, the structures of the hydrated (0001) and (1–102) surfaces of corundum have been determined recently (Eng et al., 2000; Trainor et al., 2002), and the interaction of the (0001) surface with water has been studied using synchrotron-based photoemission (Liu et al., 1998 see review by Henderson (2002) for related experimental studies) and has been modeled in several recent high-level computational chemistry studies (Hass et al., 1998; Wang et al., 2000; Lodziana et al., 2003). Therefore, we have chosen oxalate as a representative LMW organic compound and boehmite and corundum as representative Al-(oxyhydr)oxides to study the interaction of LMW organic acids with Al-bearing soil components.

We used *in situ* ATR-FTIR spectroscopy to identify the types of oxalate surface complexes and their binding modes at the boehmite/water and corundum/water interfaces. Infrared spectroscopy has long been used as a probe of adsorbate molecular structure at solid-gas interfaces, but application to environmental samples under *in situ* (wet) conditions has been limited until recently, due to interference from strong water absorption. However, improvements in the attenuated total reflection (ATR) technique have extended the application of IR spectroscopy to the qualitative study of wet environmental samples (Hind et al., 2001; Ryczkowski, 2001). Moreover, in spite of several factors complicating quantitative analysis in suspensions, such as (1) accurate subtraction of strong water absorption, and (2) correction for particle dispersivity resulting from coagulation and flocculation of charged particles (Hug and Sulzberger, 1994), this technique has become one of the most promising *in situ* probes of metal oxide/aqueous solution interfaces (e.g., Connor and McQuillan, 1999; Connor et al., 1999). Recently, ATR-FTIR has been used to study the adsorption of carboxylate molecules, including oxalate, on various metal oxide surfaces, including TiO_2, ZrO_2, Al_2O_3, Ta_2O_3, Cr_2O_3, and γ-AlOOH (Degenhardt and McQuillan, 1999; Dobson and McQuillan, 1999; Duckworth and Martin, 2001). However, as Dobson and McQuillan (1999) pointed out, the detailed coordination geometry for inner-sphere complexes, such as monodentate, end-on bidentate, and side-on bidentate, cannot be determined from infrared spectroscopy alone, implying the need for additional tools to complement IR spectroscopic observations. As a result, there have been complementary theoretical studies aimed at more detailed interpretation of ATR-FTIR spectra of carboxylic acids on metal hydroxides. Of particular relevance to the present study, Axe and Persson (2001) have recently used quantum chemical methods at the density functional theory (DFT) level to predict IR spectral frequencies of aqueous Al(III)-oxalate species, and to interpret ATR-FTIR spectra of oxalate adsorbed on boehmite. To infer the bonding geometry of adsorbed oxalate at the boehmite/water interface, they carried out frequency calculations using the gas-phase $[Al(C_2O_4)(H_2O)_4]^+$ molecule and compared the resulting frequencies with those from the IR spectrum of the aqueous $[Al(C_2O_4)(H_2O)_4]^+$ species. This comparison, and the similarity of the spectra of the aqueous $[Al(C_2O_4)(H_2O)_4]^+$ and the adsorbed oxalate species (that were probed at pH = 5.0 and

6.5, and oxalate surface coverages, 71, of 0.57 and 2.83 μmoles/m^2) allowed Axe and Persson to propose a likely complexation structure for the inner-spherically adsorbed oxalate anions.

The main purposes of the present study are to build upon the previous study of Axe and Persson (2001) by (1) determining the type(s) of oxalate species present at the boehmite/water interface as a function of a broader range of oxalate concentrations (Γ = 0, 0.25, 0.62, 1.23, 2.47, 4.93 and 16.44 μmoles/m^2) using *in situ* ATR-FTIR spectroscopy at pH = 2.5 and 5.1, and (2) obtaining more detailed structural information on the adsorbed oxalate species based on geometry optimizations and vibrational frequency calculations using quantum chemical methods on more realistic model clusters representing the aluminum oxide surface. In undertaking the latter analyses, we have utilized a cluster-based model for the mineral surface rather than a single Al atom, as was done by Axe and Persson (2001). This cluster model involved addition of multiple layers of Al and O shells around the surface Al atom, which resulted in better simulation of the environment of oxalate coordinating surface Al atoms in aluminum oxyhydroxide minerals as well as better agreement between observed and calculated oxalate vibrational frequencies, and thus a higher sensitivity to different types of oxalate binding modes on boehmite. We have also carried out similar, but more limited, ATR-FTIR studies of oxalate adsorbed at the corundum (α-Al_2O_3)/water interface, that have resulted in very similar spectra and interpretations. However, the primary focus here is on the boehmite/oxalate/water system because of its greater environmental significance. In addition, substantially higher spectral intensities were experimentally obtained for the boehmite/oxalate/water interface compared with the corundum/oxalate/water system, allowing a more quantitative interpretation of the FTIR data.

2.. EXPERIMENTAL METHODS

2.1. Chemicals and Solutions

All solutions were made from deionized water, and the background electrolyte used for all ATR-FTIR experiments was 0.01 mol/L NaCl (Mallinckrodt, AR Grade). Oxalate stock solution was prepared by dissolving sodium oxalate (Sigma, ACS reagent grade) in 0.01 mol/L NaCl. Boehmite (γ-AlOOH) used in this study was purchased from Condea Chemie GmBH and characterized using BET surface area measurements (BET area 270 m^2/g) and X-ray diffraction (XRD) analysis. Corundum (α-Al_2O_3, AKP-30) powder, with mean diameter of 0.30 μm and a BET surface area of 7 m^2/g, was purchased from Sumitomo Co. Ltd. Stock suspensions consisting of 30 g/L boehmite or 67 g/L corundum were prepared in 0.01 mol/L NaCl.

2.2. ATR-FTIR Spectroscopy

ATR-FTIR spectra were collected with a Nicolet FT-IR spectrometer (NEXUS470), equipped with a deuterated triglycine sulfate (DTGS) detector. All samples were analyzed as liquids (i.e., oxalate in aqueous solution) or wet pastes (i.e., oxalate adsorbed on α-Al_2O_3 (corundum) powder or γ-AlOOH (boehmite) powder) using the attenuated total reflection (ATR) technique. All spectra were recorded with a horizontal ATR accessory equipped with a Ge or amorphous material transmitting infrared radiation (AMTIR) crystal. Solution samples were directly applied to the ATR-FTIR crystal, and adsorption samples were prepared as follows. Aliquots of boehmite or corundum stock suspension were added to 25 mL polycarbonate centrifuge tubes. Then, oxalate stock solution (0.2 mol/L) was added to achieve a desired concentration, and the pH of the suspension was adjusted to the desired value using HCl and NaOH solutions. Samples were rotated end-over-end for 24 to 36 h while pH was readjusted every 12 h. To separate and concentrate the pastes, 30 to 60 min centrifugation at 10,000g centrifugal force was carried out for each sample. After centrifugation, the supernatant was decanted and the wet pastes were uniformly applied directly to the Ge or AMTIR crystals, with a small volume of the decanted supernatant being applied on top of this layer. A lid was placed over the crystal to protect the samples from drying during data collection. Typically, 200 to 500 scans were collected per sample and averaged. For each sample, 0.01 mol/L NaCl solutions with the same pH (2.5 or 5.1) were prepared, and their ATR-FTIR spectra were also collected. These spectra were subtracted from the sample spectra to remove the strong contributions from water bands. In the case of corundum, a strong signal due to physisorbed water was removed by further subtracting the signal from a corundum paste measured at the same pH, but in the absence of oxalate. All data collection and spectral calculations were performed using OMNIC (version 6.0a, Nicolet Instrument Corp.) and GRAMS (version 5.03, Galactic Industries Corp.) software.

In our experiments, an oxalate solution concentration of $\sim$ 10 mM or greater was required to obtain a sufficiently strong IR signal to detect. For samples in which oxalate ions are adsorbed on boehmite particles, the detection sensitivity for the adsorbed species will depend on the surface area and diffusivity of the wet paste, but the minimum concentration of oxalate in the sample volume illuminated by the IR beam should be the equivalent of 10 mM. Therefore, use of solid samples with high surface area is required for samples with low oxalate loading.

2.3. Dissolution Measurements

Limited boehmite dissolution measurements were performed as a function of oxalate concentration using a simple batch-type methodology. Briefly, aliquots of boehmite stock suspension and oxalate solutions of appropriate concentration were added to polypropylene centrifuge tubes to achieve a wide range of final oxalate concentrations (0–27 μmol/m^2) and a common boehmite concentration of 12 g/L. The pH of the suspension was adjusted to the desired value (pH = 2.5 or 5.0), and samples were rotated end-over-end for 48 h in all cases. During this period, the pH was monitored and regularly readjusted to the target pH condition by addition of small volumes of 1 to 10 mol/L HCl and NaOH. Samples were then centrifuged for 30 to 60 min at a centrifugal force of 10,000g, with the supernatant being decanted and passed through a 20 nm syringe filter. Finally, the filtered supernatants were analyzed for dissolved aluminum using inductively coupled plasma (ICP) spectrometry.

2.4. Computational Methods

Quantum chemical geometry optimization and IR vibrational frequency calculations were performed on oxalate and on Al_8O_{12} and $Al_{14}O_{22}$ clusters with and without adsorbed oxalate using the GAUSSIAN 98 program (Frisch et al., 1998) at the Hatree-Fock (HF) and B3LYP hybrid DFT levels of theory with the 6–31+G* and 6–31+G*/3–21G basis sets. These calculations differ from those of Axe and Persson (2001) who used gas-phase models of Al-oxalate to simulate the interaction of aqueous oxalate anions with the boehmite surface. The HF and B3LYP raw frequency values were corrected using a scale factor of 0.8929 for HF (Pople et al., 1993) and 0.9613 for B3LYP (Wong, 1996). The optimized structures were determined without symmetry constraints on any of the molecules. Stationary points were identified as true minima of the molecular potential energy surfaces because no imaginary frequencies were found for the optimized structures.

As described in section 3.2.1, the IR spectral features of oxalate adsorbed on both corundum and boehmite powders are very similar (see Table 3), indicating that oxalate has a similar adsorption geometry on both substrates. The (0001) surface of corundum was chosen as the substrate for model cluster calculations because this surface has been studied extensively using modern theoretical and experimental methods, and its surface structure (Hass et al., 1998; Eng et al., 2000; Wang et al., 2000) and stability (Lodziana et al., 2003) have been determined in hydrous environments. Moreover, Wittbrodt et al. (1998) used the Al_8O_{12} cluster as a model to study the interaction of water with the α-Al_2O_3 (0001) surface. We have constructed Al_8O_{12} (Fig. 2b) and $Al_{14}O_{22}$ clusters (Fig. 2c) for

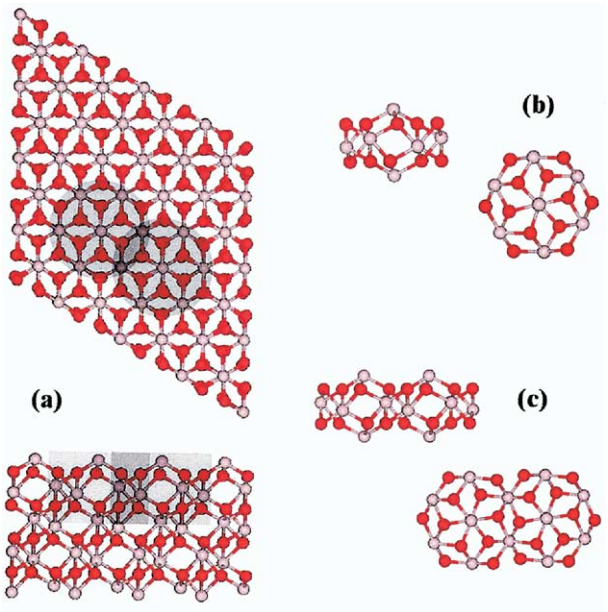

Fig. 2. Top and side view (a) Al-terminated α-Al_2O_3 (0001) surface, (b) Al_8O_{12}, and (c) $Al_{14}O_{22}$ clusters. Clusters (b) and (c) were extracted from the regions represented by the shaded circles and rectangles in (a). The lighter gray circles represent aluminum cations, whereas the darker gray circles represent oxygen ions.

use as model substrates by extracting atoms around a likely adsorption site on the corundum (0001) surface (Fig. 2a) as a starting point for geometry optimization before the interaction of this surface with oxalate and water. To simulate the α-Al_2O_3 (0001) surface, we relaxed the surface atoms of the top-most layer and fixed the structure of the subsurface atoms to their bulk crystal positions. Consequently, only the central AlO_3 group atoms on the surface and adsorbate are optimized, while the coordinates of the other atoms are frozen to prevent unrealistically large relaxation into space that is occupied by the bulk crystal in the actual system. Additionally, a split basis set was applied to the system as a compromise between the computational time and accuracy of the calculation. The optimized atoms were treated with the 6–31+G* basis set, while other frozen atoms were described by the smaller 3–21G basis set.

3. RESULTS AND DISCUSSION

3.1. Oxalate in Aqueous Solution

Figure 3a shows ATR-FTIR spectra of various oxalate species in aqueous solutions with different pH values. Considering the pK_a values for oxalate (see Table 1) and the IR spectral features observed in Figure 3a, the dominating species at near-neutral pH (see Fig. 3a spectra at pH 6.30 and 5.63) is oxalate (Ox^{2-}), whereas hydrogen oxalate (HOx^-) is dominant in the slightly acidic region (see Fig. 3a spectra at pH 3.34 and 2.76), and oxalic acid (H_2Ox) becomes significant in very acidic solutions (see Fig. 3a spectrum at pH 1.42). The observed IR spectra for Ox^{2-} species are composed of only two strong peaks (1309 cm^{-1} and 1571 cm^{-1}) stemming from symmetric (υ^s_{co}) and asymmetric (υ^a_{co}) vibrations, respectively, of the carboxylate functional group (Nakamoto, 1997). In contrast, the ATR-FTIR spectra of protonated species (hydrogen oxalate/oxalic acid) show more complex features due to the breakdown of molecular symmetry of oxalate as a result of protonation. To test the quantitative capability of this ATR-FTIR technique, we decomposed the spectra taken at pH values between 2.76 and 6.30 into Ox^{2-} and OxH^- species, and from this decomposition,

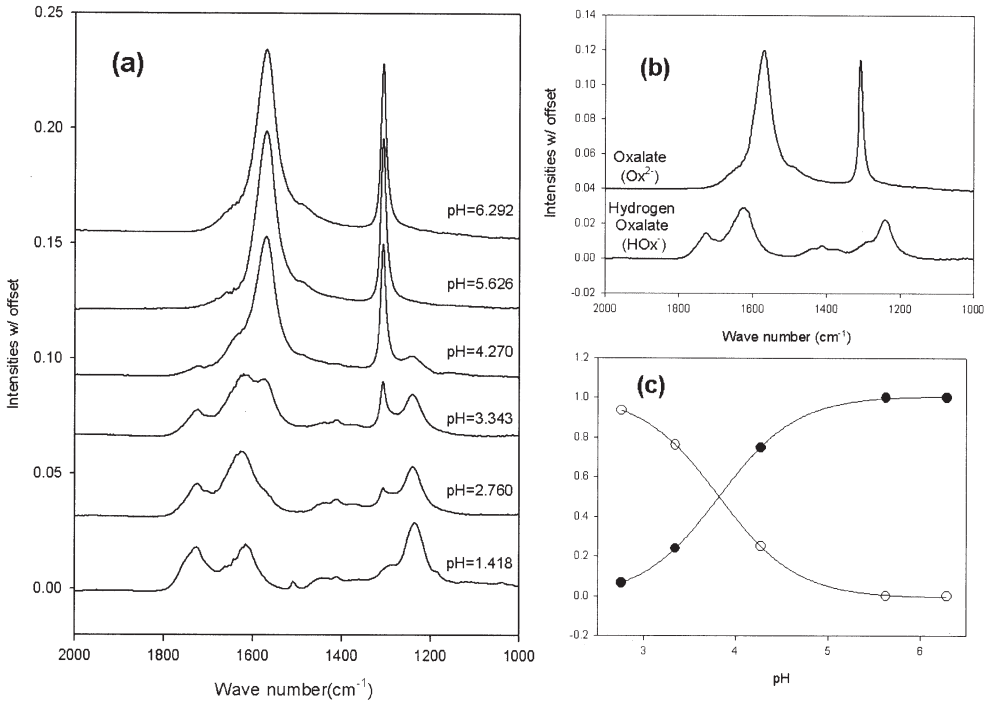

Fig. 3. (a) ATR-FTIR spectra of aqueous oxalate/hydrogen oxalate/oxalic acid system at different solution pH values; (b) Infrared spectra of aqueous oxalate and hydrogen oxalate species extracted from spectra shown in (a); and (c) Plot of aqueous oxalate (open circles) and hydrogen oxalate (solid circles) species distribution over the pH range 2.76 to 6.30. Each spectrum in (a) is referenced to a different 0 point.

Table 1. pK_{a1} and pK_{a2} values of oxalate for various solution concentrations (at 25°C).

Solution conditions	pK_{a1}	pK_{a2}
25°, 0 M	1.25*	4.27*
25°, 0.1 M	1.04*	3.82*
25°, 0.5 M	1.02*	3.55*
25°, 0.6 M	0.97**	3.57**
25°, 1.0 M	1.04*	3.55*
25°, 3.0 M	1.26*	3.80*
25°, 0.01 M	—	3.82***

* Martel and Smith (1974).
** Sjoberg and Ohman (1985).
*** This study.

pH dependent species distribution curves (see Fig. 3c) and the pKa_2 of Ox^{2-}/OxH^- were obtained. The pKa_2 value estimated from these spectroscopic measurements is 3.82, which is in good agreement with the literature values listed in Table 1.

Compared with the Ox^{2-} species, the spectral features of OxH^- are more complex and include at least 6 peaks within the measured spectral range, which might complicate interpretation of FTIR spectra of adsorbed oxalate species. Therefore, our initial ATR-FTIR experiments and quantum chemical simulations focused on adsorbed oxalate species at pH 5.1, where oxalate is the dominant species, and then were extended to acidic conditions, where HOx^- is dominant.

As mentioned in the introduction, we also used a quantum chemical approach involving geometry optimization and vibrational frequency calculations to help interpret the IR spectra. The geometry of oxalate (Ox^{2-}) was optimized in the gas phase, and vibrational frequencies were calculated and compared with observed spectral features. The calculated symmetric (υ^s_{co}) and asymmetric (υ^a_{co}) vibrational frequencies of oxalate at different levels of theory and the difference ($\Delta\upsilon$) between them are compared with the experimentally observed frequencies of aqueous oxalate species in Table 2. These comparisons show that experimental and theoretical results match reasonably well, even for the "gas phase" oxalate calculations (the differences between the experimentally observed and calculated $\Delta\upsilon$ values are only -2% for HF/6–31+G* and 10% for HF/6–31G**). However, because these calculations were conducted in the gas phase rather than an aqueous environment, it is necessary to check the effect of water solvation in the aqueous environment. Particularly for molecules with polar functional groups such as carboxylates, solvation with highly polar water molecules might have significant influences on observed physical properties. This solvation effect can be simulated by addition of explicit water molecules and/or application of self-consistent reaction field (SCRF) methods (e.g., Onsager, polarized continuum model (PCM), and self-consistent isodensity polarized continuum model (SCIPCM); Foresman et al., 1996). We applied the Onsager and PCM methods to oxalate as shown in Table 2. However, for calculations using 6–31+G* and 6–31G** basis sets at the HF level, application of SCRF methods and explicit water addition did not improve the fit with experimental frequencies relative to the gas phase calculations for oxalate. Recently, Axe and Persson (2001) also reported similar observations for oxalate in aqueous solutions using B3LYP/6–31G* methods. Additionally, calculations using higher level theory (B3LYP) did not significantly improve agreement between theory and experiment in the present study. Therefore, here we have employed HF/6–31+G* level theory without explicit water molecules or SCRF methods to predict the coordination geometry of oxalate species adsorbed on Al_8O_{12} and $Al_{14}O_{22}$ clusters (see Section 3.2.3 below).

Table 2. Comparison of observed and calculated oxalate vibrational frequencies (numbers in parenthesis are the differences between the calculated and experimentally observed aqueous oxalate frequencies).

Observed frequencies	υ^a_{co}	υ^a_{co}	$\Delta\upsilon$	Method Employed
Aqueous Oxalate	1309	1571	262	
Oxalate adsorbed in outer-sphere mode	1314	1591	277	
Calculated frequencies	υ^a_{co}	υ^a_{co}	$\Delta\upsilon$	
HF/6–31 + G*				
Oxalate	1286 (−23)	1543 (−28)	257 (−5)	Gas phase
Oxalate + $2H_2O$	1295 (−14)	1544 (−27)	249 (−13)	Gas phase
HF/6–31G**				
Oxalate	1308 (−1)	1598 (+27)	290 (+28)	Gas phase
Oxalate + $2H_2O$	1312 (+3)	1589 (+18)	277 (+15)	Gas phase
Oxalate	1293 (−16)	1579 (+8)	286 (+24)	SCRF (Onsager)
Oxalate + $2H_2O$	1296 (−13)	1578 (+7)	282 (+20)	SCRF (Onsager)
B3LYP/6–31 + G*				
Oxalate	1272 (−37)	1566 (−5)	294 (+32)	Gas phase
Oxalate + $2H_2O$	1280 (−29)	1561 (−10)	281 (+19)	Gas phase
Oxalate	1298 (−11)	1533 (−38)	235 (−27)	SCRF (PCM)
B3LYP/6–31G**				
Oxalate	1272 (−37)	1566 (−5)	294 (+32)	Gas phase
Oxalate + $2H_2O$	1280 (−29)	1561 (−10)	281 (+19)	Gas phase
Oxalate	1257 (−52)	1550 (−21)	293 (+31)	SCRF (Onsager)
Oxalate + $2H_2O$	1263 (−46)	1553 (−18)	290 (+28)	SCRF (Onsager)

HF = Hatree-Fock; SCRF = self-consistent reaction field. PCM = polarized continuum model.

Table 3. Comparison of FTIR peak positions for oxalate adsorbed on various metal oxide surfaces.

Adsorption System	υ_1	υ_2	υ_3	υ_4	References
Oxalate + TiO_2	1271	1424	1686	1711	Dobson and McQuillan (1999)
Oxalate + ZrO_2	1284	1432	1673	1708	Dobson and McQuillan (1999)
Oxalate + Al_2O_3	1297	1424	1695	1720	Dobson and McQuillan (1999)
Oxalate + Ta_2O_5	1266	1406	1688	1711	Dobson and McQuillan (1999)
Oxalate + Cr_2O_3	1276	1407	1682	1708	Degenhardt and McQuillan (1999)
Oxalate + γ-AlOOH	1288	1413	1702	1722	Axe and Persson (2001)
$[Al(C_2O_4)(H_2O)_4]^+$	1281	1412	1706	1725	Axe and Persson (2001)
$[Al(C_2O_4)_3]^{3-}$	1272/1308	1405	1697	1720	Axe and Persson (2001)
Oxalate + α-Al_2O_3	1294	1425	1699	1720	This work
Oxalate + γ-AlOOH					
Species A	1286	1418	1700	1720	This work
Species B	1297	1408	1697	1721	This work

3.2. Oxalate Adsorbed on Al-(oxyhydr)oxide Surfaces

3.2.1. Spectroscopic determination of oxalate speciation at corundum/water and boehmite/water interfaces at pH 5.1

We conducted ATR-FTIR measurements on wet pastes consisting of corundum/oxalate/water at pH 5.1 (spectra not shown). As indicated in Table 3, new peaks at 1720, 1699, 1425, and 1294 cm^{-1} were observed at $\Gamma_{ox} = 1.4$ μmoles/m^2, suggesting the formation of adsorbed oxalate species. However, in the case of corundum powder, the complicated background subtraction procedures due to the signals from physisorbed water and/or hydroxyl groups at the interface, and the lack of an internal reference peak to normalize the dispersivities of corundum particles, made quantitative speciation analysis of the corundum/oxalate/water system difficult. Therefore, similar measurements were made for oxalate adsorbed at the solid/solution interface of a boehmite powder with a substantially higher surface area and enhanced adsorption capacity relative to the corundum powder originally used. As a consequence, the boehmite/oxalate/water spectra had much stronger signals from adsorbed oxalate species (see Fig. 4a). Moreover, boehmite is thermodynamically more stable than corundum under hydrous conditions (Navrotsky, 2001), reducing the potential for complications arising from phase transformations and requiring a much simpler background subtraction procedure compared to corundum powder for the quantitative IR analysis of oxalate species.

To correct for effects caused by the dispersed nature of boehmite particles, including charging effects induced by oxalate sorption, that can result in significant differences in boehmite surface area in the sample volume penetrated by the IR beam, we normalized all IR spectra of the sorption samples relative to the height of the boehmite feature at 1157 cm^{-1}. As mentioned in the introduction, appropriate correction for charging effects and particle dispersivities is one of the main issues affecting peak intensities in ATR FTIR analysis of these types of samples (Hug and Sulzberger, 1994). In past ATR-FTIR studies of similar sorption samples, an immobile film of particles on the ATR crystal was typically prepared by drying an aqueous suspension of the particles in contact with the ATR crystal; an aqueous solution containing the adsorbate of interest was then flowed over the sample until no change in FTIR signal was detected and spectra were then collected (Hug and Sulzberger, 1994; Degenhardt and McQuillan, 1999; Dobson and McQuillan, 1999). However, this approach may not properly simulate *in situ* conditions quantitatively because the sorbent may change by forming strong aggregate with each other upon drying, and the extent of reaction between sorbate and sorbent may not be the same as when the sorption sample is prepared before deposition on the ATR crystal. As can be seen in Figure 4a, there are peaks from aqueous oxalate at 1309 and 1571 cm^{-1} and from adsorbed oxalate species on boehmite at 1286, 1418, 1700, and 1720 cm^{-1}, which are very similar to those observed for the corundum/oxalate/water samples (Table 3). In addition, there is also a peak due to boehmite at 1157 cm^{-1}. Using this boehmite peak as an internal reference, we were able to quantitatively measure the relative distribution of various aqueous and adsorbed oxalate species in this system as a function of pH and oxalate concentration.

In the IR spectra of boehmite/oxalate/water and corundum/oxalate/water samples, the observed peak positions for both mineral/water interfaces are similar (less than 17 cm^{-1} difference, see Table 3). This is an interesting observation because one might expect spectral differences in light of the different bulk structures of the two sorbents. Moreover, these observations coupled with recently published FTIR spectral data on oxalate-metal oxide complexes suggest a more general interpretation of IR spectra of adsorbed oxalate species. As shown in Table 3, the frequency differences of ATR-FTIR spectral features for a particular vibrational motion observed in this study and also by Degenhardt and McQuillan (1999), Dobson and McQuillan (1999), and Axe and Persson (2001) for the adsorbed oxalate species on TiO_2, ZrO_2, α-Al_2O_3, γ-AlOOH, Ta_2O_5, and Cr_2O_3surfaces are relatively small (less than 26 cm^{-1} difference, see Table 3), irrespective of the type of metal oxide surface on which oxalate adsorbs. Clearly, these deviations in peak positions between oxalate molecules adsorbed at various mineral substrates are minor when compared to the dramatic changes in peak positions and number of peaks caused by the oxalate adsorption process. Such observations imply that oxalate species adsorbed on various metal oxide and oxyhydroxide surfaces probably have similar coordination structures, and that the type of metal cations to which oxalate anions coordinate has a minor influence on the IR vibration frequencies of adsorbed oxalate. The latter finding is not surprising given the relatively small differences in electronegativity (χ) of the cations involved [$\chi(Ti^{4+}) = 1.32$; $\chi(Zr^{4+}) = 1.22$; $\chi(Al^{3+}) = 1.47$; $\chi(Ta) = 1.33$; and $\chi(Cr^{3+}) = 1.56$] (Allred and Rochow, 1958)

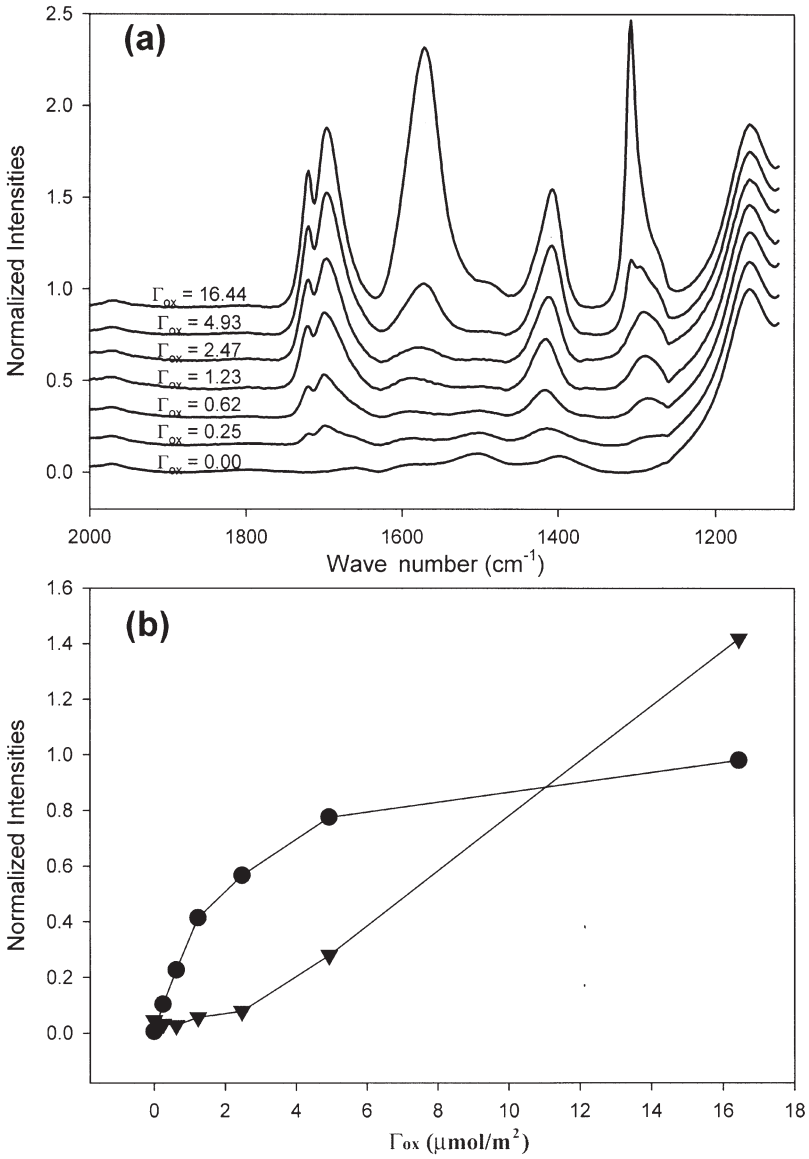

Fig. 4. (a)-ATR-FTIR spectra of oxalate species sorbed at the boehmite/water interface for various [oxalate]/[boehmite] ratios at pH 5.1. All spectra were normalized to the boehmite peak at 1157 cm^{-1}; (b) Plot of normalized intensities of peaks at 1700 cm^{-1} (filled circles) and 1571 cm^{-1} (filled triangles) corresponding to inner-sphere adsorbed and aqueous oxalate species, respectively.

and the anticipated small differences in inductive effects caused by these different cations. The results reported in Table 3 are therefore consistent with the expected minor effect of the electronic configurations of coordinating cations on the vibrational frequencies of the oxalate ligand when compared to the much more significant impact of molecular symmetry changes caused by inner-sphere oxalate adsorption.

In a previous study, the FTIR peaks located near 1286, 1418, 1700, and 1720 cm^{-1} were assigned to the adsorbed oxalate species bound in inner-sphere mode on boehmite (Axe and Persson, 2001). In the present study, however, we found that more than one species contributes to these peaks. As can be seen in Figure 5, the peaks at 1286 and 1418 cm^{-1} are shifted to 1297 and 1408 cm^{-1}, respectively, as Γ_{ox} increases, indicating the presence of at least two distinct, but structurally similar oxalate species over the Γ_{ox} range examined. Species "B," with narrower peaks positioned at 1297 and 1408 cm^{-1}, seems to be dominant at high $\Gamma_{ox,}$ while species "A", with broader peak at 1286 and 1418 cm^{-1}, seems to be dominant at low Γ_{ox}. We postulate that both species are inner-sphere oxalate species with similar coordination modes, but they are coordinated to Al cations in different environments. Based on the peak shapes, Γ_{ox} dependences, and comparisons with FTIR results previously reported by Axe and Persson (2001), species "A" is assigned to oxalate adsorbed in an inner-sphere fashion to the boehmite surface, and species "B" is assigned to oxalate coordinated to Al(III) cations in solution. The latter species (which are likely to consist of a combination of several different aqueous Al(III)-oxalate complexes with similar oxalate-binding geometries over the broad range of oxalate concentra-

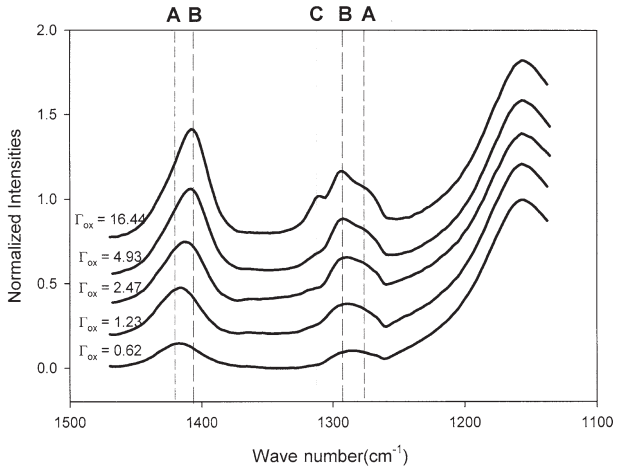

Fig. 5. ATR-FTIR spectra of oxalate species at the boehmite/water interface for various [oxalate]/[boehmite] ratios at pH 5.1, with the aqueous oxalate component at 1571 cm^{-1} removed (see Fig. 3(b)). Species "A" is oxalate adsorbed to the boehmite surface in an inner-sphere mode, species "B" is oxalate coordinated to aqueous Al(III) cations, and species "C" is outer-sphere adsorbed oxalate species.

tions investigated in this study) becomes progressively more important as the concentration of oxalate increases, and is generated by the oxalate-promoted dissolution of the boehmite surface (see Fig. 6).

In addition to these inner-sphere oxalate species, we also observed an additional adsorbed species at $\Gamma_{ox} = 0$ μmoles/m^2. In Figure 4a, the two broadened peaks located near 1397 and 1504 cm^{-1} were observed even in the absence of oxalate, and the intensities of these peaks decreased and disappeared as Γ_{ox} increased. We assign these peaks to adsorbed carbonate (Bargar et al., 1999), which is weakly bound to the boehmite surface and can be easily displaced by the strongly adsorbing oxalate anions.

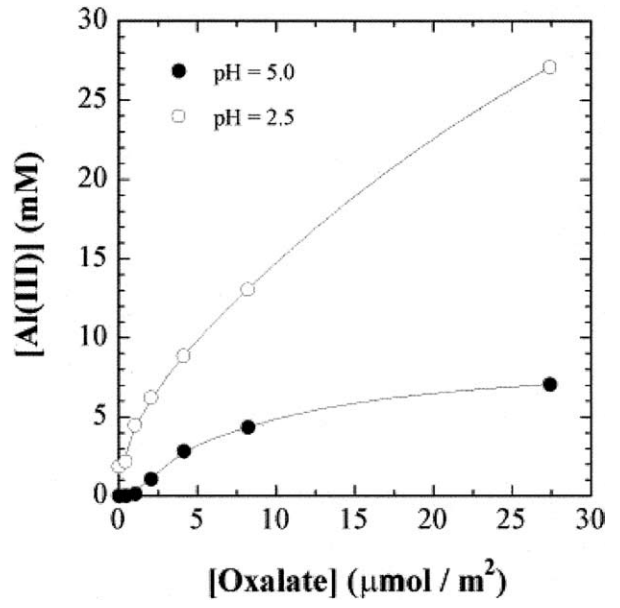

Fig. 6. Concentration of Al(III) dissolved from the boehmite surface as a function of oxalate concentration at two pH values. The equilibration time was 48 hr, and the boehmite concentration was 12 g/l in all cases.

Another interesting aspect of the spectra shown in Figure 4a is the presence of features due to additional oxalate species (e.g., oxalate bound to boehmite in outer-sphere mode). As shown in Figure 4a, a broadening and shift of the aqueous oxalate species peak at 1571 cm^{-1} to a higher wave number (1591 cm^{-1}) is observed at low oxalate surface coverages. The narrower peak, which is dominant at high Γ_{ox}, is clearly due to the aqueous oxalate species, while the broadened and shifted peak at low Γ_{ox} is best assigned to an "outer-sphere" surface complex (i.e., to oxalate ions interacting with the specific boehmite surface hydroxyl groups through weak hydrogen bonding interactions). Axe and Persson (2001) have reported similar observations, and they also ascribed these changes of peak shape and position to the asymmetric solvation effect on oxalate anions adsorbed in an outer-sphere mode. We also assign this broadened and shifted peak at 1591 cm^{-1} to the asymmetric (υ^a_{co}) vibration of the oxalate molecule, which is weakly bound to the boehmite surface in outer-sphere mode. In addition, we can expect that there might be a peak from the symmetric (υ^s_{co}) vibration of the same species near 1309 cm^{-1}, but it is difficult to clearly observe this peak due to its low intensity and large overlap with other peaks near this frequency. Therefore, to reduce the complexities in this spectral region, we subtracted the aqueous oxalate spectral component at 571 cm^{-1} (see Fig. 3b) from these spectra. Following this subtraction and peak deconvolution procedure for the spectral region presented in Figure 5a, a symmetric (υ^s_{co}) vibration associated with an outer-sphere bound oxalate species is clearly visible at 1314 cm^{-1} (species "C"), and at least two different inner-sphere oxalate species (i.e., species "A" and "B") are also revealed.

From the above observations, we have identified at least five different species present at or near the boehmite/water interface and offer the following explanation for the Γ_{ox}-dependent spectral changes. In the absence of the oxalate anion ($\Gamma_{ox} = 0$), carbonate anions are adsorbed on the boehmite surface (1397 and 1504 cm^{-1}) and are the dominant adsorbed species. When relatively small amounts of oxalate anions ($\Gamma_{ox} < 2.47$) are added to this boehmite/water sample, strongly adsorbing inner-sphere oxalate anions replace the adsorbed carbonate species through ligand exchange reactions (species "A"; 1286, 1418, 1700, and 1720 cm^{-1}), while a very small portion of oxalate anions bind weakly to boehmite in an outer-sphere mode (species "C"; 1309 and 1591 cm^{-1}). Initially, the inner-spherically adsorbed oxalate is most likely to bind to high-energy defect sites (probably singly coordinated, positively charged groups such as $AlOH^{0.5+}$) rather than the stable, electrically neutral Al_2OH or Al_4O groups that are present on the dominant (010) cleavage plane of boehmite. This is predominantly due to both the relative ease of ligand-substitution for a surface hydroxyl that is bound to only one surface cation (i.e., the lower activation energy associated with cleaving one versus two or more surface Al-O bonds) and the mononuclear nature of the inner-sphere oxalate surface complex (see Section 3.2.3). It should be noted that gradual oxalate-promoted or (at low pH) proton-promoted cleavage of Al_2OH groups may also occur and would result in additional surface sites suitable for inner-sphere adsorption of oxalate. Under the latter circumstance, a gradual transition from outer-sphere to inner-sphere adsorption modes

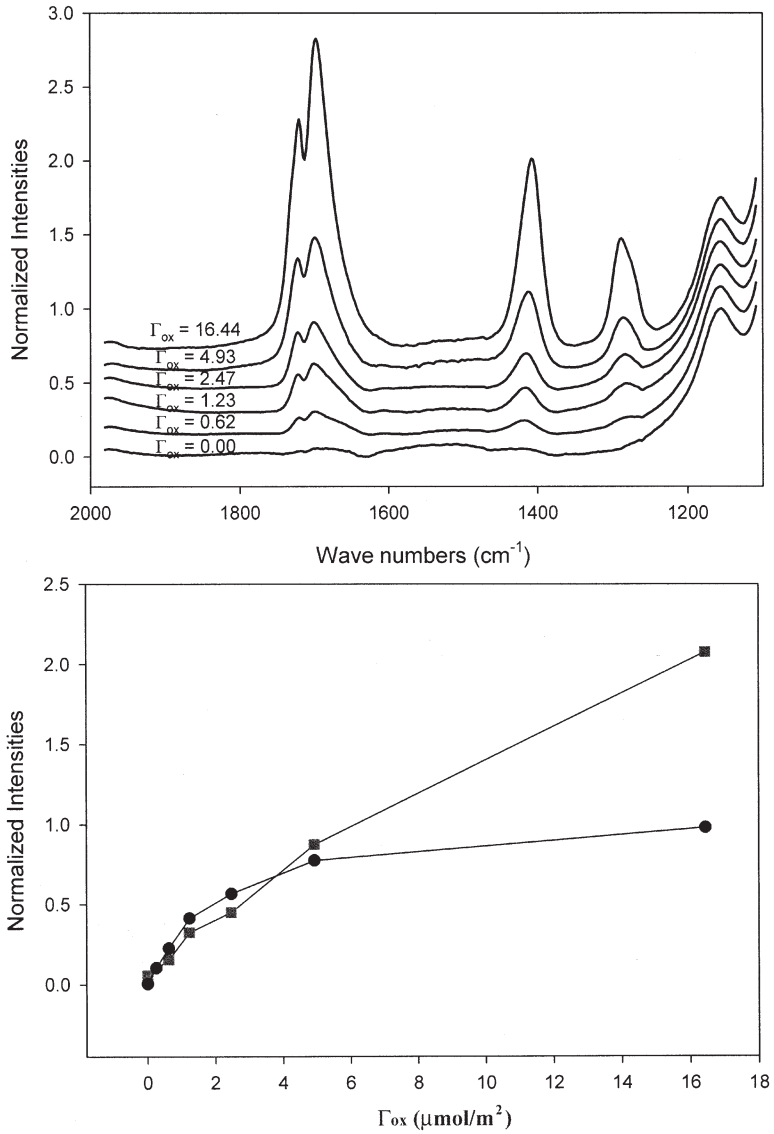

Fig. 7. (a) ATR-FTIR spectra of oxalate species at boehmite/water interface for various [oxalate]/[boehmite] ratios at pH 2.5. All spectra were normalized to the boehmite peak at 1157 cm^{-1}; (b) Plot of normalized peak intensities at 1697 cm^{-1} from IR spectra at pH 5.1 (filled circles) and pH 2.5 (filled squares) corresponding to inner-sphere oxalate species.

would be expected as a function of increasing equilibration time, a result that has recently been reported by Axe and Persson (2001). At still higher oxalate concentrations ($\Gamma_{ox} >$ 2.47), the boehmite surface binding sites for the inner-sphere coordination of oxalate become saturated (see Fig. 4b), binding site density on the boehmite surface was estimated to be 2.8 μmol/m^2 (Laiti and Ohman, 1996), and excess oxalate is present dominantly as aqueous oxalate species in the diffuse swarm of ions (i.e., at the outer Helmholtz plane and beyond) as indicated by the shift in the asymmetric carboxylate stretch from 1591 to 1571 cm^{-1} and the much smaller IR absorption at 1591 cm^{-1}, which is due to outer-sphere oxalate complexes. Outer-sphere oxalate adsorption would be less favored at this high oxalate loading because the boehmite surface charge becomes less positive due to inner-sphere oxalate adsorption. Outer-sphere adsorption is most likely to occur through hydrogen bonding interactions involving surface Al_2OH groups rather than the $AlOH^{0.5+}$ defect sites that promote inner-sphere oxalate adsorption. In addition to these adsorption processes, oxalate-promoted dissolution of boehmite, following inner-sphere adsorption of oxalate, becomes more dominant as Γ_{ox} increases (see Fig. 6), resulting in the formation of one or more aqueous Al(III)-oxalate species that are revealed by the shifted peaks at high Γ_{ox} (aqueous species "B"; 1297, 1408, 1697, and 1721 cm^{-1}). It is noteworthy that species "B" is present only at high oxalate concentrations in the systems we studied, which may explain why other studies of oxalate sorption on Al-(oxyhydr)oxides and other metal oxides have not observed it in the IR spectra they have reported (cf. Axe and Persson, 2001; Dobson and McQuillan, 1999).

In addition to the inner-sphere and outer-sphere species discussed above, we have also considered the potential presence of

Table 4. Comparisons of observed frequencies of inner-sphere oxalate at the corundum/water interface and calculated frequencies (cm^{-1}) for the geometry-optimized oxalate-Al_xO_y model clusters.

	Adsorbed species	$\upsilon_1(\Delta\upsilon_1^*)$	$\upsilon_2(\Delta\upsilon_2^*)$	$\upsilon_3(\Delta\upsilon_3^*)$	$\upsilon_4(\Delta\upsilon_4^*)$
Calculated frequencies	C_2O_4-Al_8O_{12} model (a)	1294 (0)	1437 (+12)	1684 (−15)	1717 (−3)
	C_2O_4-Al_8O_{12} model (b)	1263 (−31)	1442 (+17)	1616 (−83)	1683 (−37)
	C_2O_4-Al_8O_{12} model (c)	1318 (+24)	1473 (+48)	1597 (−102)	1640 (−80)
	C_2O_4-$Al_{14}O_{22}$ model (d)	1227 (−67)	1391 (−34)	1630 (−69)	1659 (−61)
Observed frequencies	Inner-sphere oxalate surface complex at the corundum/water interface	1294	1425	1699	1720
	Inner-sphere oxalate surface complex at the boehmite/water interface (species "A").	1286	1418	1700	1720

* Difference between the calculated and observed frequencies for oxalate adsorbed in inner-sphere mode at the corundum/water interface.

Al-oxalate precipitates at the boehmite/water interface. The existence of such species would be expected to result in distinct IR spectral features corresponding to altered bonding environments of oxalate in the precipitate phase. To test for such a possibility, the IR spectrum of crystalline $Al_2(C_2O_4)_3$ was measured and compared with the spectra shown in Figure 4a. No correlation was found between the major features of the spectra of $Al_2(C_2O_4)_3$ and adsorbed oxalate, indicating that precipitate phases are, at most, present as very minor species under our experimental conditions.

3.2.2. *Spectroscopic determination of oxalate speciation at the boehmite/water interface at pH 2.5*

We also carried out ATR-FTIR measurements on the boehmite/oxalate/water system at pH 2.5, where hydrogen oxalate (HOx^-) is the dominant species in aqueous solution and the boehmite surface is more positively charged (pH_{pzc} is ~8.5; Sverjensky, 1994). Adsorption of HOx^- species onto boehmite could potentially introduce spectral features in addition to those observed at pH 5.1. As can be seen in Figure 7a, the IR spectra of the boehmite/oxalate/water system at pH 2.5 are significantly simplified compared with those measured at pH 5.1 (see Fig. 4a). Although the experiments undertaken at pH 2.5 and 5.1 were conducted over the same Γ_{ox} ranges, at pH 2.5 there are no detectable peaks from adsorbed carbonate, aqueous Ox^{2-}/HOx^-, or outer-sphere oxalate species. Instead, only peaks corresponding to inner-sphere oxalate species (both "A" and "B" species discussed in section 3.2.1; see Fig. 8) are observed. The absence of aqueous or outer-sphere oxalate species and the continuous increase of peak intensities due to adsorbed oxalate at pH 2.5 (see Fig. 7b) suggest a significant increase in the number of surface binding sites available for inner-sphere oxalate adsorption, that is thought to be a precursor to oxalate-promoted dissolution (Furrer and Stumm, 1986). This observation can be explained as follows: (1) protonation of boehmite surface sites under acidic conditions increases the number of positively charged surface sites, that are then more vulnerable to a ligand exchange reaction by oxalate, resulting in a higher degree of oxalate adsorption compared to that at pH 5.1; and/or (2) the rapid dissolution process promoted by these high proton and/or oxalate concentrations (see Fig. 6) produces a large number of Al(III) cations and nanometer-sized Al(III)-based 'particles' (e.g., $Al_{13}O_4(OH)_{24}(H_2O)_{12}^{7+}$; see Casey and Swaddle, 2003) with a much higher effective surface area than the starting boehmite powder. These dissolution products provide significantly higher concentrations of binding sites and/or Al(III) cations, which can react with aqueous hydrogen oxalate species to form adsorbed oxalate species or aqueous Al(III)-oxalate species. In addition, the similarity of adsorbed oxalate spectral features measured at pH 2.5 and 5.1 suggests that the coordination geometries of adsorbed oxalate species at both pH values are similar. From this observation we also suggest that the adsorption mechanism of aqueous HOx^- involves the loss of a proton during the ligand-exchange adsorption reaction or during the transfer process from bulk solution to the mineral/water interface. We conclude that the adsorbed species formed under acidic conditions have very similar (or the same) coordination structures as the adsorbed species formed at pH 5.1.

3.2.3. *Quantum chemical calculations of infrared vibrational frequencies and identification of inner-sphere oxalate at boehmite/water and corundum/water interfaces*

From the larger peak shifts in IR spectral features ascribed to adsorbed oxalate species, compared with those of other carboxylate ligands with outer-sphere coordination (e.g., phthalate and pyromellitate (Yoon and Brown, 2001)), as well as the splitting of the two IR peaks of aqueous oxalate into four peaks of adsorbed oxalate, we conclude that oxalate adsorbed at the boehmite/water and corundum/water interfaces has a substantially different molecular geometry than aqueous oxalate (i.e.,

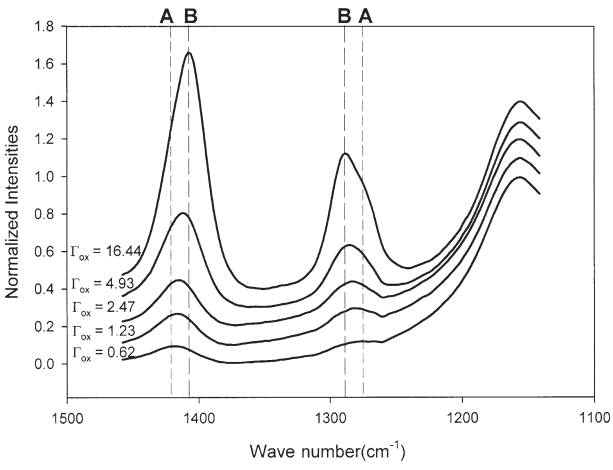

Fig. 8. ATR-FTIR spectra of oxalate species at the boehmite/water interface for various [oxalate]/[boehmite] ratios at pH 2.5. Species "A" is oxalate adsorbed to the boehmite surface in an inner-sphere mode, and species "B" is oxalate coordinated to aqueous Al(III) cations.

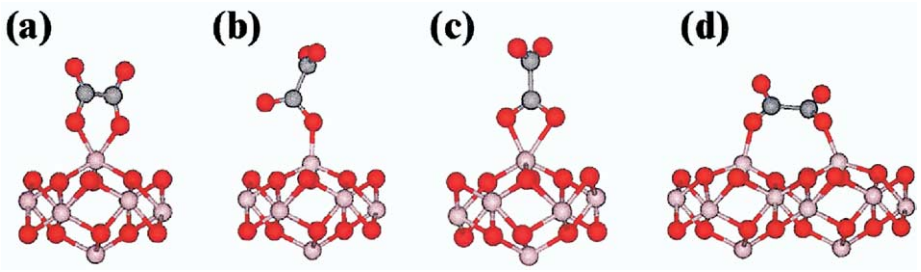

Fig. 9. Side view of four possible inner-sphere coordination structures for oxalate-Al_8O_{12} (a)–(c) and oxalate-$Al_{14}O_{22}$ (d) clusters: (a) a bidentate side-on structure with a 5-membered ring resulting in an Al surface site that is 5-coordinated; (b) a monodentate end-on structure resulting in an Al surface site that is 4-coordinated; (c) a bidentate end-on structure with a 4-membered ring resulting in an Al surface site that is 5-coordinated; and (d) a bidentate binuclear structure resulting in two Al surface sites that are 4-coordinated. The lighter gray circles in the Al_8O_{12} cluster represent aluminum cations, whereas the darker gray circles represent oxygen ions. In the adsorbed oxalate molecule, the lighter gray circles represent carbon atoms, whereas the darker gray circles represent oxygens. Geometries were optimized at the HF/6–31+G* (3–21G) level using Gaussian 98 (Frisch et al., 1998).

inner-sphere coordination to the mineral surface causes a lowering of the high molecular symmetry of aqueous oxalate). However, we cannot speculate further about the geometry or mode of binding of adsorbed oxalate from these spectroscopic observations alone, in agreement with the conclusions of Dobson and McQuillan (1999), who carried out similar experiments. Therefore, we have carried out quantum chemical calculations for adsorbed oxalate in various coordination geometries. As discussed in section 3.1, we have previously shown that geometry optimization and frequency calculations using quantum chemical methods result in IR spectra that closely match the observed results for aqueous oxalate species. However, for oxalate species adsorbed on mineral surfaces, an appropriate model of the sorbent surface is required to attain a realistic simulation of the vibrational frequencies of adsorbed oxalate. Axe and Persson (2001) used vibrational frequencies derived from density functional calculations on Al(III)-oxalate model complexes to assign the IR peaks of oxalate adsorbed on boehmite (γ-AlOOH); however, the "gas phase" Al(III)-oxalate model complexes considered were not found to accurately reproduce the observed vibrational frequencies of adsorbed oxalate. In contrast, our calculations have used Al_8O_{12} and $Al_{14}O_{22}$ clusters as substrates for oxalate adsorption, and geometry optimization and IR vibrational frequency calculations have been carried out using several possible adsorbed oxalate coordination geometries to identify the most likely structure of adsorbed oxalate molecules.

We tested four possible coordination structures for the oxalate-Al_xO_y clusters, including: (a) mononuclear bidentate side-on coordination of oxalate with a 5-membered ring, that results in a 5-coordinated Al surface site; (b) monodentate end-on coordination of oxalate, that results in a 4-coordinated Al surface site; (c) mononuclear bidentate end-on coordination of oxalate with a 4-membered ring, that results in a 5-coordinated Al surface site; and (d) binuclear bidentate coordination of oxalate, that results in two 4-coordinate Al surface sites (see Fig. 9). From the frequency calculations using optimized structures of models (a) through (d), we obtained four distinct IR-active vibrational frequencies from each adsorbed oxalate molecule in the spectral range 2000 to 1000 $cm^{-}1$ (see Table 4). As can be seen in Table 4 and Figure 10, the calculated frequencies for model (a) most closely match the experimental observations from the boehmite/oxalate/water and corundum/oxalate/water systems, while the simulation results for models (b), (c), and (d) show large deviations. Based on this comparison, the most probable coordination geometry for oxalate adsorbed on aluminum (oxyhydr)oxides is bidentate side-on coordination resulting in a 5-membered ring. The vibrational modes associated with this complex are shown diagrammatically in Figure 11.

Interestingly, as has been previously discussed (see Section 3.2.1), deviations between the calculated frequencies among differently coordinated oxalate molecules are substantially larger (maximum of 91 cm^{-1}) than the deviations among experimentally observed frequencies of oxalate molecules adsorbed at various mineral surfaces (maximum of 26 cm^{-1}: see Table 3). Such findings strongly suggest that the oxalate coordination structures at various mineral surfaces are likely to be very similar to the complexation structure (bidentate side-on coordination to form a 5-membered chelate ring) that exists for the corundum/oxalate/water system.

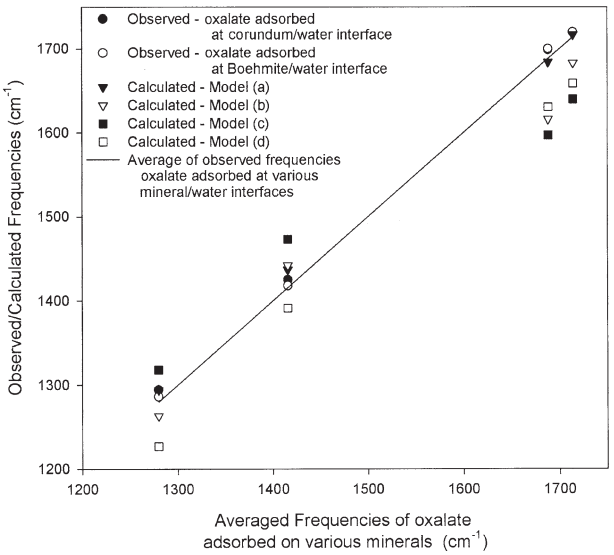

Fig. 10. Comparison of observed infrared frequencies for oxalate sorbed on corundum and boehmite with the calculated frequencies for the four oxalate-Al_8O_{12} and oxalate-$Al_{14}O_{22}$ models.

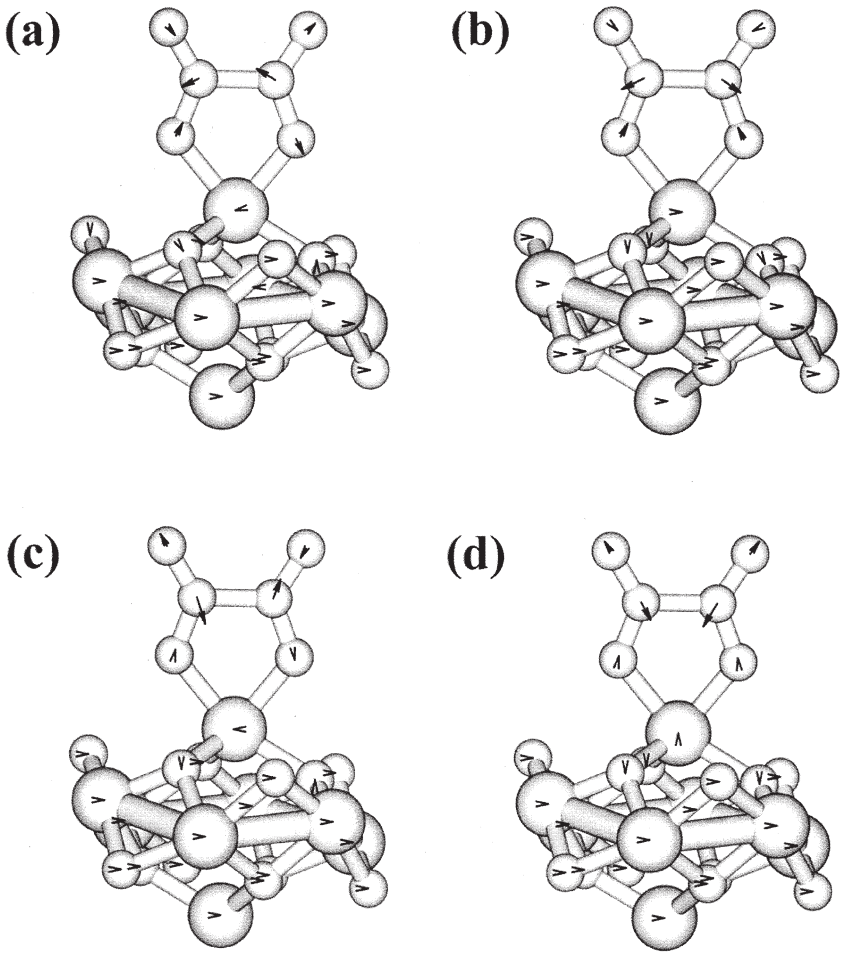

Fig. 11. Vibrational modes of oxalate adsorbed in a "bidentate side-on coordination with 5-membered ring" corresponding to the adsorbed oxalate species peaks observed at (a) 1286, (b) 1418, (c) 1700, and (d) 1720 cm^{-1}. The lengths of arrows are proportional to the atomic displacements of selected normal modes.

It is noteworthy that the Al site in the model (a) Al_8O_{12} cluster to which oxalate bonds is coordinated to five oxygen atoms rather than six following oxalate adsorption (see Figs. 1a and 9a). This local coordination for Al in our geometry-optimized cluster contrasts with the results of a recent crystal truncation rod (CTR) diffraction study of the hydrated α-Al_2O_3 (0001) surface, where surface Al atoms are 6-coordinated by oxygen atoms and/or hydroxyl ions (Eng et al., 2000). However, the hydrated α-Al_2O_3 (0001) surface was free of any adsorbate other than water in the CTR study. To further examine this difference in Al coordination, we modified the model (a) cluster by adding a hydroxyl group (model (a′)) or water molecule (model (a″)) to the first coordination shell of Al such that the reactive Al site becomes 6-coordinated (see Fig. 12). We found, however, that geometry optimization of these clusters using quantum chemical optimization methods did not result in convergence to a minimum energy structure. More specifically, geometry optimization of the model (a′) cluster with an additional hydroxyl group coordinating Al at the oxalate binding site resulted in the dissociation of Al-$O_{substrate}$ bonds, while the model (a″) cluster with an additional water molecule coordinating Al at the oxalate binding site resulted in dissociation of the Al-O_{water} bond, yielding a 5-coordinated Al at the surface binding site. This apparent preference for 5-coordinated Al at the interface can also be rationalized using the bond valence model of Brown (2002). For model (a), the sum of the bond valences to the surface aluminum is 2.84 v.u., which is in better agreement with Pauling's electrostatic valence principles (Pauling, 1929) than the bond valence sums for model (a′) or model (a″), which are 3.84 v.u. and 3.34 v.u., respectively (assuming the following bond valences (s): s(Al-$O_{substrate}$) = 0.5 v.u., s(Al-$O_{oxalate}$) = 0.67 v.u., s(Al-$O_{hydroxyl}$) = 1.0 v.u., and s(Al-O_{water}) = 0.5 v.u.). This simple bond valence analysis also suggests that the 5-coordinated Al at the interface could form stable bonds with two oxygens from the oxalate molecule.

Kubicki (2001) recently predicted the presence of 5-coordinated Al(III), Fe(III), and Si(V) in aqueous solution based on HF and DFT calculations using the supermolecule approach (i.e., explicit hydration) combined with self-consistent reaction field methods. During the Al(III) hydrolysis simulations, significant structural changes were observed as deprotonation of first-shell water molecules occurred. More

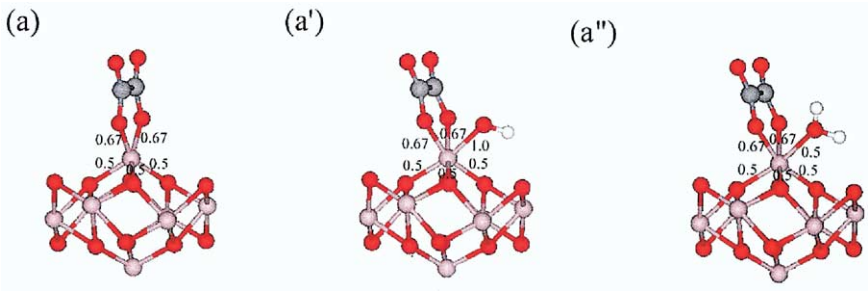

Fig. 12. Side view of three modified model structures for oxalate-Al_8O_{12}: (a) a bidentate side-on structure with a 5-membered ring resulting in an Al surface site that is 5-coordinated; (a′) modification of structure (a) with an additional OH group bonded to the surface Al resulting in a 6-coordinated Al site; (a″) modification of structure (a) with an additional water molecule bonded to the surface Al resulting in a 6-coordinated Al site. The numbers are bond valences (in valence units) of each Al-O bond used to calculate the bond valence sum to Al. The lighter gray circles in the Al_8O_{12} cluster represent aluminum cations, whereas the darker gray circles represent oxygen ions. In the adsorbed oxalate molecule, the lighter gray circles represent carbon atoms, whereas the darker gray circles represent oxygens.

specifically, removal of the first three protons followed by energy minimization produced 5-coordinated Al species (i.e., $[Al(OH)_3(H_2O)_2]7H_2O$), while removal of less than two or more than four protons resulted in 6- or 4-coordinated Al species. Based on our results, we suggest that oxalate adsorption results in 5-coordinated Al(III) at boehmite/water and corundum/water interfaces under the conditions of our experiments. We also suggest that this adsorbed species occurs as an intermediate species in the oxalate-promoted mineral dissolution mechanism, perhaps caused by adsorbate-induced restructuring of the surface. However, the presence of such 5-coordinated intermediate species and the nature of the underlying dissolution mechanism(s) cannot be determined unequivocally from the quantum chemical simulations presented in the present study. Additional quantum chemical studies on more realistic systems (including the addition of explicit water/hydroxyl molecules and larger cluster sizes) are in progress.

4. CONCLUSIONS

In situ ATR-FTIR results are consistent with at least four distinct oxalate species (aqueous oxalate, outer-sphere adsorbed oxalate, inner-sphere adsorbed oxalate, and aqueous Al(III)-oxalate species) at or near the boehmite/water interface at Γ_{ox}ranging from 0.25to 16.44 μmol/m^2. The proportions of each type of oxalate species present vary as function of pH and oxalate surface coverage. Oxalate adsorbed in an inner-sphere mode is dominant at lower oxalate surface coverages ($\Gamma_{ox} < 2.47$), and the proportions of aqueous oxalate and aqueous Al(III)-oxalate species (species "B") become dominant as Γ_{ox} increases. At lower pH (2.5), aqueous Al(III)-oxalate species become more concentrated with increasing pH, indicating the predominance of oxalate- and proton-promoted dissolution of the boehmite surface. The coordination geometry of inner-sphere oxalate species was predicted using quantum chemical geometry optimization and IR vibrational frequency calculations. Geometry-optimized Al_8O_{12} and $Al_{14}O_{22}$ clusters, with the reactive surface Al sites coordinated by three oxygens, were used as model substrates for the corundum and boehmite surface binding sites. Among the four possible coordination structures considered, IR frequency calculations based on a model for adsorbed oxalate consisting of mononuclear bidentate side-on coordination with a 5-membered ring agree best with the observed IR frequencies. Our results on the inner-sphere coordination geometry of oxalate generally concur with those of Axe and Persson (2001) and Degenhardt and McQuillan (1999), but provide more direct evidence for inner-sphere oxalate coordination geometries at boehmite/water and corundum/water interfaces. Furthermore, we tentatively suggest that the resulting 5-coordinated Al(III) at the boehmite/water and corundum/water interfaces is an intermediate species in the oxalate-promoted mineral dissolution mechanism.

Acknowledgments—We wish to acknowledge the support of NSF Grant CHE-0089215 (Stanford University CRAEMS on Chemical and Microbial Interactions at Environmental Interfaces). We thank Dr. James Rustad (Pacific Northwest National Laboratory) for helpful discussions about quantum chemical calculations on the alumina clusters and three anonymous reviewers and the Associate Editor for helpful reviews. We also thank to Prof. Scott E. Fendorf (Stanford University) and Dr. Guangchao Li (Stanford University) for help with the FTIR spectroscopy.

Associate editor: C. Eggleston

REFERENCES

Allred A. L. and Rochow E. G. (1958) A scale of electronegativity based on electrostatic force. *J. Inorg. Nucl. Chem.* **5,** 264–268.

Axe K. and Persson P. (2001) Time-dependent surface speciation of oxalate at the water-boehmite (γ-AlOOH) interface: Implications for dissolution. *Geochim. Cosmochim. Acta* **65,** 4481–4492.

Bargar J. R., Reitmeyer R., and Davis J. A. (1999) Spectroscopic confirmation of uranium(VI)-carbonato adsorption complexes on hematite. *Environ. Sci. Technol.* **33,** 2481–2484.

Boily J. F., Nilsson N., Persson P., and Sjoberg S. (2000a) Benzenecarboxylate surface complexation at the goethite (α-FeOOH)/water interface: I. A mechanistic description of pyromellitate surface complexes from the combined evidence of infrared spectroscopy, potentiometry, adsorption data, and surface complexation modeling. *Langmuir* **16,** 5719–5729.

Boily J. F., Persson P., and Sjoberg S. (2000b) Benzenecarboxylate surface complexation at the goethite (α-FeOOH)/water interface: III. The influence of particle surface area and the significance of modeling parameters *J. Colloid Interface Sci.* **227,** 132–140.

Brown G. E. Jr. and Parks G. A. (2001) Sorption of trace elements from aqueous media: Modern perspectives from spectroscopic studies and comments on adsorption in the marine environment. *Int. Geol. Rev.* **43,** 963–1073.

Brown I. D. (2002) *The Chemical Bond in Inorganic Chemistry-The Bond Valence Model. IU. Cr monographs on Crystallography 12.* Oxford University Press.

Casey W. H. and Swaddle T. W. (2003) Why small?. The use of small inorganic clusters to understand mineral surface and dissolution reactions in geochemistry *Rev. Geophys.* **41,** 4/1–4/20.

Connor P. A. and McQuillan A. J. (1999) Phosphate adsorption onto TiO_2 from aqueous solutions: An in situ internal reflection infrared spectroscopic study. *Langmuir* **15,** 2916–2921.

Connor P. A., Dobson K. D., and McQuillan A. J. (1999) Infrared spectroscopy of the TiO_2/aqueous solution interface. *Langmuir* **15,** 2402–2408.

Davis J. A. (1982) Adsorption of natural dissolved organic matter at the oxide/water interface. *Geochim. Cosmochim. Acta* **46,** 2381–2393.

Davis J. A. (1984) Complexation of trace metals by adsorbed natural organic matter. *Geochim. Cosmochim. Acta* **48,** 679–691.

Degenhardt J. and McQuillan A. J. (1999) Mechanism of oxalate ion adsorption on chromium oxide-hydroxide from pH dependence and time evolution of ATR-IR spectra. *Chem. Phys. Let.* **311,** 179–184.

Dobson K. D. and McQuillan A. J. (1999) In situ infrared spectroscopic analysis of the adsorption of aliphatic carboxylic acids to TiO_2, ZrO_2, Al_2O_3, and Ta_2O_5 from aqueous solutions. *Spectrochim. Acta Part A* **55,** 1395–1405.

Duckworth O. W. and Martin S. T. (2001) Surface complexation and dissolution of hematite by C-1-C-6 dicarboxylic acids at pH = 5.0 *Geochim. Cosmochim. Acta* **65,** 4289–4301.

Eick M. J., Peak J. D., and Brady W. D. (1999) The effect of oxyanions on the oxalate-promoted dissolution of goethite. *Soil Sci. Soc. Am. J.* **63,** 1133–1141.

Eng P. J., Trainor T. P., Brown G. E., Jr., Waychunas G. A., Newville M., Sutton S. R., and Rivers M. L. (2000) Structure of the hydrated α-Al_2O_3 (0001) surface. *Science* **288,** 1029–1033.

Foresman J. B., Frisch A., and Gaussian Inc. (1996) *Exploring Chemistry with Electronic Structure Methods.* Gaussian Inc.

Frisch M. J., Trucks G. W., Schlegel H. B., Scuseria G. E., Robb M. A., Cheeseman J. R., Zakrzewski V. G., Montgomery J. J. A., Stratmann R. E., Burant J. C., Dapprich S., Millam J. M., Daniels A. D., Kudin K. N., Strain M. C., Farkas O., Tomasi J., Barone V., Cossi M., Cammi R., Mennucci B., Pomelli C., Adamo C., Clifford S., Ochterski J., Petersson G. A., Ayala P. Y., Cui Q., Morokuma K., Malick D. K., Rabuck A. D., Raghavachari K., Foresman J. B., Cioslowski J., Ortiz J. V., Baboul A. G., Stefanov B. B., Liu G., Liashenko A., Piskorz P., Komaromi I., Gomperts R., Martin R. L., Fox D. J., Keith T., Al-Laham M. A., Peng C. Y., Nanayakkara A., Gonzalez C., Challacombe M., Gill P. M. W., Johnson B. B., Chen W., Wong M. W., Andres J. L., Gonzalez C., Head-Gordon M., Replogle E. S., and Pople J. A. (1998) Gaussian 98, Revision A.7.

Furrer G. and Stumm W. (1986) The coordination chemistry of weathering. 1. Dissolution kinetics of δ-Al_2O_3 and BeO *Geochim. Cosmochim. Acta* **50,** 1847–1860.

Hass K. C., Schneider W. F., Curioni A., and Andreoni W. (1998) The chemistry of water on alumina surfaces: Reaction dynamics from first principles. *Science* **282,** 265–268.

Henderson M. A. (2002) The interaction of water with solid surfaces: Fundamental aspects revisited. *Surf. Sci. Rpts.* **46,** 1–308.

Henrich V. E. and Cox P. A. (1994) *The Surface Science of Metal Oxides.* Cambridge University Press.

Hind A. R., Bhargava S. K., and McKinnon A. (2001) At the solid/liquid interface: FTIR/ATR: the tool of choice. *Adv. Colloid Interface Sci.* **93,** 91–114.

Hug S. J. and Sulzberger B. (1994) In-situ Fourier-transform infrared spectroscopic evidence for the formation of several different surface complexes of oxalate on TiO_2 in the aqueous-phase. *Langmuir* **10,** 3587–3597.

Kubicki J. D. (2001) Self-Consistent Reaction Field Calculations of Aqueous Al(III), Fe(III), and Si(IV): Calculated Aqueous-Phase Deprotonation Energies Correlated with Experimental $\ln(K_a)$ and pK_a. *J. Phys. Chem. A* **105,** 8576–8762.

Johnson S. B., Yoon T. H., Kocar B. D., and Brown G. E., Jr. (2004a) Adsorption of organic matter at mineral/water interfaces: II. Outer sphere adsorption of maleate and implications for dissolution processes. *Langmuir* (in press).

Laiti E. and Ohman L. O. (1996) Acid/base properties and phenylphosphonic acid complexation at the boehmite/water interface. *J. Colloid Interface Sci.* **183,** 441–452.

Liu P., Kendelewicz T., Brown G. E., Jr., Nelson E. J., and Chambers S. A. (1998) Reaction of water with α-Al_2O_3 and α-Fe_2O_3 (0001) surfaces: synchrotron x-ray photoemission studies and thermodynamic calculations. *Surf. Sci.* **417,** 53–65.

Lodziana Z., Norskov J. K., and Stoltze P. (2003) The stability of the hydroxylated (0001) surface of α-Al_2O_3. *J. Chem. Phys.* **118,** 11179–11188.

Martell A. E. and Smith R. M. (1974) *Critical Stability Constants.* Plenum Press.

Nakamoto K. (1997) *Infrared and Raman Spectra of Inorganic and Coordination Compounds.* John Wiley & Sons.

Navrotsky A. (2001) Thermochemistry of nanomaterials. *Rev. Mineral.* **44,** 73–103.

Nordin J., Persson P., Laiti E., and Sjoberg S. (1997) Adsorption of o-phthalate at the water-boehmite (γ-AlOOH) interface: Evidence for two coordination modes. *Langmuir* **13,** 4085–4093.

Nordin J., Persson P., Nordin A., and Sjoberg S. (1998) Inner-sphere and outer-sphere complexation of a polycarboxylic acid at the water-boehmite (γ-AlOOH) interface: A combined potentiometric and IR spectroscopic study. *Langmuir* **14,** 3655–3662.

Pauling L. (1929) The principles determining the structure of complex ionic crystals. *J. Am. Chem. Soc.* **51,** 1010–1026.

Persson P., Nordin J., Rosenqvist J., Lovgren L., Ohman L. O., and Sjoberg S. (1998) Comparison of the adsorption of o-phthalate on boehmite (γ-AlOOH), aged γ-Al_2O_3, and goethite (α-FeOOH). *J. Colloid Interface Sci.* **206,** 252–266.

Pople J. A., Scott A. P., Wong M. W., and Radom L. (1993) Scaling factors for obtaining fundamental vibrational frequencies and zero-point energies from HF/6–31G* and MP2/6–31G* harmonic frequencies. *Israel J. Chem.* **33,** 345–350.

Ryczkowski J. (2001) IR spectroscopy in catalysis. *Catalysis Today* **68,** 263–381.

Schnitzer M. (2000) A lifetime perspective on the chemistry of soil organic matter. *Adv. Agron.* **68,** 1–58.

Sjoberg S. and Ohman L. O. (1985) Equilibrium and structural studies of silicon(IV) and aluminum(III) in aqueous-solution. 13. A potentiometric and Al-27 nuclear-magnetic-resonance study of speciation and equilibria in the aluminum(III) oxalic-acid hydroxide system *J. Chem. Soc. -Dalton Trans.* **12,** 2665–2669.

Strobel B. W. (2001) Influence of vegetation on low-molecular-weight carboxylic acids in soil solution. A review. *Geoderma.* **99,** 169–198.

Stumm W. (1987) *Aquatic Surface Chemistry: Chemical Processes at the Mineral-Water and Particle-Water Interface in Natural Systems.* Wiley-Interscience.

Sverjensky D. A. (1994) Zero-point-of-charge prediction from crystal chemistry and solvation theory. *Geochim. Cosmochim. Acta* **58,** 3123–3129.

Trainor T. P., Eng P., Brown G. E., Jr., Robinson I. K., and De Santis M. (2002) Crystal truncation rod diffraction study of the clean and hydrated α-Al_2O_3 (1–102) surface. *Surf. Sci.* **496,** 238–250.

Vaughan D. J. and Wogelius R. A. (2000) *Environmental Mineralogy*. Eötvös University Press. Budapest, Hungary.

Wang X.-G., Chaka A., and Scheffler M. (2000) Effect of the environment on the α-Al_2O_3 (0001) surface structures. *Phys. Rev. Lett.* **84,** 3650–3653.

White A. F. and Brantley S. L. (ed.) (1995) Chemical Weathering Rates of Silicate Minerals. In *Reviews in Mineralogy*, Vol. 31, Mineralogical Society of America.

Wittbrodt J. M., Hase W. L., and Schlegel H. B. (1998) *Ab initio* study of the interaction of water with cluster models of the aluminum terminated (0001) alpha-aluminum oxide surface. *J. Phys. Chem. B.* **102,** 6539–6548.

Wong M. W. (1996) Vibrational frequency prediction using density functional theory. *Chem. Phys. Lett.* **256,** 391–399.

Yoon T. H. and Brown G. E., Jr. (2001) ATR FR-IR spectroscopic studies on the 1, 2, 4, 5-benzenetetracarboxylate bound to water/goethite (α-FeOOH) interface. *Abstracts of Papers of the American Chemical Society* **222 (pt.1),** U444-U444.

Yoon T. H., Johnson S. B., and Brown G. E., Jr. (2004) Adsorption of Suwannee River fulvic acid on aluminum oxyhdroxide surfaces: an in situ ATR-FTIR study. *Langmuir* **20** 5655-5658.

Zinder B., Furrer G., and Stumm W. (1986) The coordination chemistry of weathering. 2. Dissolution of Fe(III) oxides *Geochim. Cosmochim. Acta* **50,** 1861–1869.